Fizika Nizkikh Temperatur, 1997, v. 23, Nos. 5/6, p. 586–597

On the properties of vacancies in solid ^{4}He as studied by pressure measurements

P. Remeijer, S. C. Steel, R. Jochemsen, and G. Frossati

Kamerlingh Onnes Laboratorium, Leiden University P. O. Box 9506, 2300 RA Leiden, The Netherlands
E-mail: reyer@rulkol.leidenuniv.nl

J. M. Goodkind

Physics Department 0319, University of California at San Diego 9600 Gilman Drive, La Jolla, CA 92037, U.S.A.

Submitted November 26, 1996

We have measured the temperature dependence of the pressure at constant volume in solid ^{4}He in the low density hcp phase. The measurements are analysed in terms of a localized vacancy model and the free Bose gas model of vacancies in solid helium. The results agree better with the free Bose gas model. Within this model we have determined the effective mass of the vacancies to be 3–5 times the bare mass of a ^{4}He atom, corresponding to a bandwidth of 1.3–2.1 K.

PACS: 67.80, 66.30.L

1. Introduction

There has always been much interest in vacancies in both solid ^{3}He and ^{4}He. Due to the large zero point motion in helium a vacancy, or free lattice site, will have a high probability of tunneling to adjacent lattice sites. This distinguishes helium from other solids where the vacancies are rather localized at low temperature. When the energy of formation of a vacancy is positive, the vacancies are thermally activated and will vanish exponentially at low temperature.

Theoretical studies suggest the possibility that in quantum solids, vacancies may still exist at absolute zero temperature [1]. Due to the large mobility of the vacancies they will not have a single energy of formation, but occupy a band of energy states, the energy of formation being in the center of the band. The lower limit of the band can become negative which results in a non-zero vacancy concentration at zero temperature. In ^{4}He, these so called zero point vacancies will behave like bosons and are expected to Bose condense, thus giving the crystal superfluid-like properties.

Most experiments seeking evidence for Bose condensation of the zero point vacancies concentrated on superfluid mass flow [2–5]. No positive proof of vacancy flow was found and this has mainly been attributed to an extremely low critical speed or a very low T_c .

Van de Haar et al. [6] made an attempt to find the zero point vacancies without depending on the critical velocity by measuring the pressure between 1.5 and 120 mK. The vacancies, which are expected to behave as an interacting Bose gas, will contribute to the pressure in the solids and reveal themselves by a finite $\partial P/\partial T$ value at very low temperatures. A superfluid transition would be observed by a kink in the pressure. An upper limit to the zero point vacancy concentration $x_{zpv} \leq 6{\cdot}10^{-7}$ was determined and no sharp kinks were found, indicating a T_c lower than 1.5 mK, the lowest temperature obtained during the experiment.

In this work we concentrate on the properties of thermally activated vacancies. Although the existence of these vacancies is clear, their properties are not known. A large collection of experiments has been carried out, involving charge mobility [7–11], x-ray scattering [12], NMR [13–15], heat capacity [16] and sound attenuation [17] measurements. Large discrepancies exist between the vacancy densities and activation energies that are extracted from the various experiments, although Burns et al. [18] showed that better agreement can be found when the data is interpreted assuming that the

vacancies occupy a wide energy band (free boson model) instead of a narrow band.

We have measured the pressure of solid ^{4}He as a function of temperature for samples with molar volumes in the range of 20.908 and 20.981 cm^3 and temperatures between 0.3 K and the melting temperature of the crystals. From the data we were able to establish the existence of thermally activated vacancies and we could, within the framework of the free Bose gas model, extract the effective mass and the activation energy of the vacancies.

2. Theoretical models on vacancies in ^{4}He

We will give an overview of two common models that have been proposed to describe the vacancies. The first model presented treats the vacancies as localized phenomena or classical lattice defects with an activation energy Φ. The second model describes the opposite case of completely delocalized vacancies. In this case, the vacancies will behave like a free Bose gas with effective mass M. Finally the contribution of the phonons to the pressure will be discussed.

Localized vacancies

When looking at vacancies from a classical point of view we can visualize them as being static crystal defects which are localized in the lattice. The (configurational) entropy will then be given by the possible configurations of putting n vacancies in a lattice of N ^{4}He atoms:

$$S_c = k_B \ln\left(\frac{(N+n)!}{N!\,n!}\right), \tag{1}$$

which can be simplified by using Stirling's formula to

$$S_c = k_B\left[n \ln\left(\frac{N+n}{n}\right) + N \ln\left(\frac{N+n}{N}\right)\right]. \tag{2}$$

The equilibrium number of vacancies can be found by minimizing the free energy of this system:

$$F = F_0 + nf - TS_c\,, \tag{3}$$

where F_0 is the free energy of the lattice without vacancies and f is the free energy of a single vacancy. Using the fact that N is of the order of Avogadro's constant and $n << N$ we find

$$x = \frac{1}{e^{f/k_BT} - 1} \approx e^{-f/k_BT} \tag{4}$$

with the vacancy concentration $x = n/N$, and the last simplification being only true for temperatures low compared to the vacancy free energy. With the further definition of

$$f = \Phi - Ts\,, \tag{5}$$

where s is the entropy change of the crystal due to the introduction of one single vacancy, the vacancy creation energy or activation energy Φ has been related to the vacancy concentration x. In practice this non-configurational entropy s turns out to be rather small [12], meaning that f and Φ are virtually equivalent.

Since in our experiments we measure pressure as a function of temperature it is necessary to know the pressure contribution of the vacancies. The total pressure of a system is given by expression

$$P = -\left(\frac{\partial F}{\partial V}\right)_T. \tag{6}$$

In our case we can calculate the vacancy part of the pressure by using the vacancy free energy part of F which yields

$$P_{\text{vac}} = -n\left(\frac{\partial f}{\partial V}\right)_T =$$

$$= -N\left(\frac{\partial \Phi}{\partial V} - T\frac{\partial s}{\partial V}\right) e^{-\Phi/k_BT}\, e^{s/k_B}\,. \tag{7}$$

The volume dependence of the activation energy has been studied by Lengua et al. [17]. From their data we can calculate for the molar volumes of interest here that

$$N\left(\frac{\partial \Phi}{\partial V}\right) \approx -4.5\cdot 10^8 \text{ Pa}\,. \tag{8}$$

So this model provides a means of determining the magnitude of the activation energy and the vacancy formationentropy.

The free Bose gas model

The large quantum behavior of ^{4}He has the consequence that the tunneling probability for a vacancy to hop to an adjacent site is large. This mobility will lead to a band of energy states. In the case that the width of the band (Δ) is large compared to the temperature, the vacancies will behave like a free Bose gas. The great canonical partition function is given by

$$\Xi = \sum_{N=0}^{\infty} \sum_{\mathbf{k}} \frac{1}{N!} \exp\left(\frac{\mu N - E_{\mathbf{k}}}{k_BT}\right). \tag{9}$$

The dispersion relation in the case $\Delta >> T$ is equal to the dispersion relation of free bosons with an activation energy Φ and is given by

$$E_{\mathbf{k}} = \Phi + \frac{\hbar^2 \mathbf{k}^2}{2M} \tag{10}$$

with the vacancy activation energy Φ sometimes called the gap of the energy band, and the effective mass of the vacancies M. The sum over all $\mathbf{k}$ values in the great canonical partition function may be replaced by an integral over E. Using the density of states

$$\rho(E) = \frac{V}{(2\pi)^2}\left(\frac{2M}{\hbar^2}\right)^{3/2}(E-\Phi)^{1/2}\,, \tag{11}$$

we then find for the vacancy concentration

$$x = \frac{1}{N} k_B T \int_{\Phi}^{\infty} \frac{\rho(E)}{e^{E/k_B T} - 1}\, dE =$$

$$= \frac{V}{N}\left(\frac{M}{2\pi\hbar^2}\right)^{3/2} (k_B T)^{3/2} g_{3/2}\left(e^{-\Phi/k_B T}\right) \tag{12}$$

and for the pressure due to the vacancies

$$P = \frac{2}{3V} \int_{\Phi}^{\infty} \frac{E\rho(E)}{e^{E/k_B T} - 1}\, dE =$$

$$= \left(\frac{M}{2\pi\hbar^2}\right)^{3/2} (k_B T)^{5/2} g_{5/2}\left(e^{-\Phi/k_B T}\right) \tag{13}$$

with the polylog function g_σ defined as

$$g_\sigma(z) = \frac{1}{\Gamma(\sigma)} \int_0^{\infty} \frac{x^{\sigma-1}}{z^{-1}e^x - 1}\, dx\,. \tag{14}$$

As one can see, the model provides direct access to the effective mass M and the activation energy Φ. In the tight-binding approximation, the effective mass is directly correlated to the bandwidth Δ of the energy spectrum by

$$M = \frac{6\hbar^2}{a^2 \Delta} \tag{15}$$

with a as the atomic distance. If the activation energy is large compared to the temperature and the bandwidth ($\Phi >> k_B T$, Δ), the free Bose gas model with the effective mass replaced by the bandwidth according to Eq. (15), becomes equivalent to a narrow band model as described by various authors [19,20].

The phonon contribution

In order to be able to study the vacancy contribution to the pressure it is necessary to calculate the magnitude and temperature dependence of the phonon background pressure. The thermodynamic properties of solid ^{4}He have been extensively studied by Gardner et al. [16] and we will use their results to make an estimate of the phonon contribution to the pressure. They found that the constant volume heat capacity C_v can be described in very good approximation by a Debye T^3 term supplemented by a T^7 term.

The Grüneisen parameter γ links the heat capacity to the pressure by

$$\frac{\alpha}{C_v} = \gamma \frac{B}{V}\,, \tag{16}$$

α is the coefficient of expansion; B is the bulk modulus and V is the volume.

Using the reciprocity theorem we get

$$\left(\frac{\partial P}{\partial T}\right)_V = -\left(\frac{\partial V}{\partial T}\right)_P \left(\frac{\partial V}{\partial P}\right)_T^{-1} = \frac{\alpha}{B}\,, \tag{17}$$

which in combination with (16) yields

$$\left(\frac{\partial P}{\partial T}\right)_V = \gamma \frac{C_v}{V} = \frac{\gamma}{V}\left(AT^3 + CT^7 + \ldots.\right). \tag{18}$$

In the low temperature limit ($T << \Theta_D$, with $\Theta_D \cong 27$ K for ^{4}He) the Grüneisen parameter is only slightly temperature dependent, which means that simple integration of the last expression yields a pressure term that will only depend on T^4 and T^8 terms. With the coefficients A and C of Gardner et al. [16], converted to SI units, and $\gamma \cong 2.8$ this yields

$$P = 0.07 \frac{A(V_m)}{V_m} T^4 + 0.035 \frac{C(V_m)}{V_m} T^8\,. \tag{19}$$

3. Experimental setup

A copper platform (10 cm in diameter, thickness 0.6 cm) served as a single temperature mounting plate on which the cell, a germanium thermometer, a fixed point device, a heater, and a carbon resistor thermometer (CRT) were placed. This platform was attached to the mixing chamber cold plate using Vespel SP21 [21] rods, posing a heat leak of less

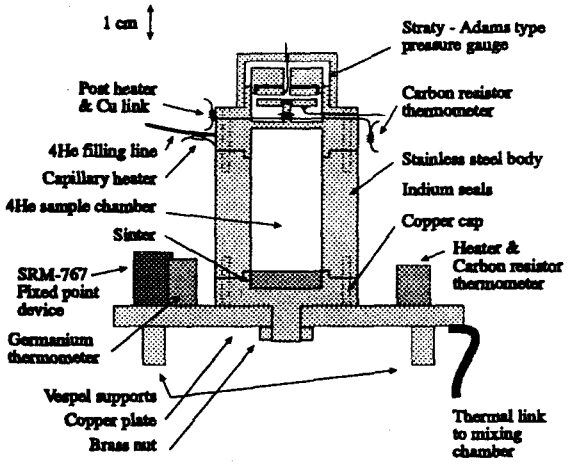

Fig. 1. The constant volume cell placed on the copper platform. The post- and capillary heaters can be seen near the top.

than 2.5 μW to the mixing chamber, with the platform at a temperature of 1 K.

A thermal link was provided by means of a carefully calculated copper wire (Ø 2.0 mm, length 45 mm, standard electrolytic quality) connected between the platform and the mixing chamber coldplate. It was chosen such that 5 mW of heating power would maintain a temperature of 1 K on the platform.

The constant volume cell, depicted in Fig. 1 was made as rigid as possible. To obtain this, the body was made of a 1 cm thick stainless steel cylinder. The low end was closed with a copper cap containing the silver sinter. The stainless steel top cap contained the Straty–Adams type pressure gauge. The ^{4}He volume formed this way measured Ø 2 cm×4 cm, 12 cm^3. The cell was clamped onto the copper plate with a brass nut.

The sinter was made with 7.6 grams XRP-5 powder [22], of which the surface area is estimated to be 0.76 m^2 [23].

A Straty–Adams [24] type strain gauge was incorporated into the cell to measure pressure. The thin stainless steel top wall of the cell served as the flexible membrane for the gauge. One of the capacitor electrodes of the gauge was glued to the post connected to this membrane using Stycast 2850FT [25]. The second electrode was glued in position while resting against the bottom plate, with the cell pressurized to 2.7 MPa. This procedure guarantees a very small distance between the plates for pressures lower than 2.7 MPa, the "gluing pressure", thereby giving a high sensitivity. Electrical connections to the electrodes were fed through small holes in the cell wall. Coaxial cables were used to minimize stray capacitance effects.

The gauge was calibrated at 1 K against a Degranges & Huot dead weight tester [26]. The standard deviation of the fit to the calibration points was less than 50 Pa. The random error in the pressure, introduced through the capacitance measurement of the strain gauge, is smaller than 2 Pa when using the Andeen Hagerling AH2500 capacitance bridge [27]. The pressure of the ^{4}He melting curve minimum, $P_{min} = 2.53081$ MPa, was reproduced to within 100 Pa.

To ensure a homogeneous growth of the crystals we needed to have a vertical temperature gradient in the cell, the bottom being the coldest part. To enable this, a possibility to heat the post of the flexible membrane was arranged. Because of limited space near this post, the heater, a metal film resistor, was put outside the cell while thermal contact between the post and the heater was provided by a copper wire.

Due to the shallow minimum in the ^{4}He melting curve it is possible that the filling line gets blocked with solid when its temperature is close to 780 mK. To overcome this undesirable effect a second heater was connected to the ^{4}He filling line.

Another heater was placed on the platform. It consisted of 50 cm manganin wire wound on a copper cylinder (10 mm in diameter) on which a carbon resistor thermometer was placed as well.

Three thermometers were placed on the platform, the SRM-767 fixed point device, a germanium, and a carbon resistor thermometer. Another carbon resistor thermometer was thermally anchored to the post that connects the top wall of the cell to the pressure gauge electrode. It was used to measure the temperature of the top of the cell (Fig. 1).

The germanium thermometer was calibrated against the SRM-767 [28] fixed point device. The maximum deviation we expect for this thermometer is 5 mK. A consistency check was made by carefully measuring the minimum of the ^{4}He melting curve. Our thermometers read 782 ± 3 mK at the minimum, which agrees quite well with earlier measurements by Grilly [29].

For controlling the temperature we used the carbon resistor thermometer located on the platform in combination with the platform heater to form a PID (Proportional Integration Derivative) feedback loop. The brain of this regulator was a Hewlett Packard HP9000/300 Unix computer in combination with a DAC (Digital Analog Converter) to drive the heater and an ADC (Analog Digital Converter) to read the temperature. Both the ADC and

the DAC were contained in a Hewlett Packard HP35650. The setup was able to maintain a temperature constant to within 0.05% and is programmable which exceedingly simplified the slow process of stepping through the whole temperature region.

Since vacancies have the tendency to bind to impurities and defects in the crystal it is important to remove these as much as possible. Commercial ^{4}He has a contamination with ^{3}He, which is typically of the order of 1 ppm. We used the heat flush effect to purify the ^{4}He gas [30,31]. A mass spectrometer check showed that the ^{3}He impurity content is significantly below 1 ppm, but on the basis of the experience of other workers, using the same technique, it is more likely that the concentration will be (far) below 1 ppb.

4. Measurements of the *P-T* relation of solid ^{4}He

All data presented here has been acquired during two cool-downs of the cell. Major improvements to the experimental setup were made after the first run however. Therefore data from the first run is mainly included for completeness.

Growing the crystals

All crystals were grown in the temperature range 1.2–1.4 K. As one can see from Fig. 2 the melting curve shows a positive slope in this temperature region. While growing the crystals the temperature of the platform and the cell pressure were kept constant. The cell pressure was chosen to coincide with the ^{4}He melting pressure corresponding to the platform temperature. Using the heater connected to the top of the cell (post-heater), a vertical gradient was introduced. In this way, slowly decreasing the vertical temperature gradient across the cell caused the solid to grow from the bottom up, and the filling line, located at the top most part of the cell, would block last.

After growing the crystal, the volume of the cell was closed by increasing the pressure a few bars above the growth pressure, thereby blocking the filling line. Subsequently, all crystals were annealed by leaving them slightly below their melting temperature during a period of 6 h.

A total of eighteen crystals of very pure ^{4}He were prepared during both runs. A number of those proved to be badly grown, the telltale being anomalous superheating below the melting curve, sudden pressure shifts or irreproducibility upon warming and cooling. We believe the main cause of this to be lack of pressure stability during growth. After thermally cycling the crystals, the reproducibility of the *P–T* relation always improved significantly, indicating that this would in fact be a better annealing method than the one that was described before. This was also found by Iwasa et al. [32] for solid ^{3}He crystals.

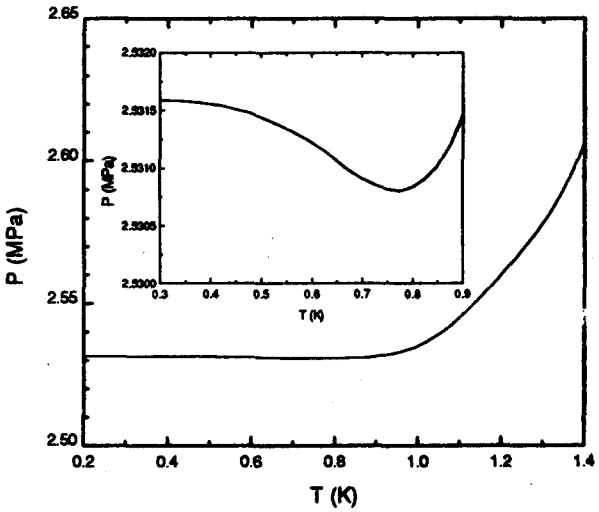

Fig. 2. The ^{4}He melting curve. The inset shows the region of the minimum. The temperature at which this minimum occurs is 780 mK and the depth is approximately 800 Pa.

Results

The *P-T* curves were measured by making small temperature steps (± 40 steps over the whole temperature region 0.2 K–1.4 K) and allowing the crystal to equilibrate at each temperature. This procedure is shown in Fig. 3.

We used stability of the pressure reading as the equilibrium condition. The time to reach equilibrium was typically 5 to 10 min, after which approximately 50 data readings were taken. Averaging reduced the noise contribution to the pressure reading by a factor 7 to 0.4 Pa. A single sweep through the temperature region would take approximately 7–10 h. Also visible in Fig. 3 is the pressure shift occurring between a warm-up measurement and a subsequent cool-down. This is due to a slow shift of the plug in the filling line, resulting in an increase of pressure and a decrease in molar volume. Therefore, only cool-downs with accompanying warm-up measurements will be at equal molar volume. All useful samples along with their melting temperature and molar volume are summarized in Table 1. The *P-T* relations are shown in Figs. 4 and 5. Despite of the smoothness of the *P-T* relation of crystal No 10 we could not use the curve for fitting, due to its

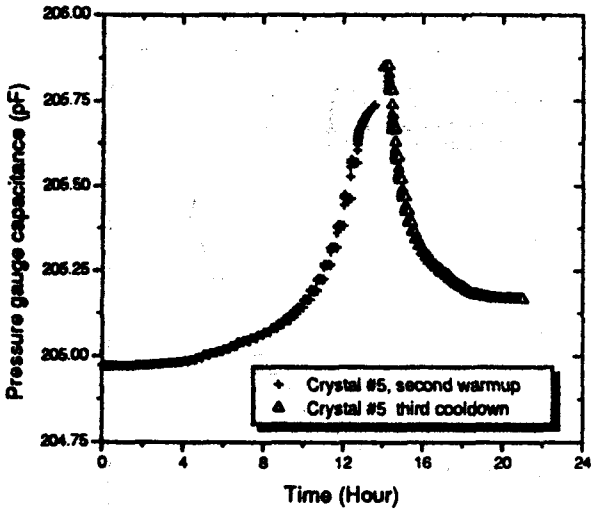

Fig. 3. The capacitance of the pressure gauge as a function of time, before averaging, for crystal No 5 during the second warm-up and the third cool-down. The capacitance (pressure) increase between the two measurements is due to a shift of the plug.

limited temperature span. The molar volumes of all samples were estimated from the limiting pressure at low temperature, using molar volume and compressibility data on hcp ^4He from Grilly [29].

Table 1

Summary of all good quality crystals that were used for fitting. Each item indicates a *P-T* curve taken upon cooling (c) or warming (w). Also shown are the crystal number and an index for future reference. The molar volumes were estimated from the limiting low temperature pressure (see text).

Crystal No	Warming / Cooling	Cycle No	Index	V_m, cm^3
3	w	1	3w1	20.981
4	c	1	4c1	20.908
4	w	1	4w1	20.908
5	c	2	5c2	20.944
5	c	3	5c3	20.940
5	w	1	5w1	20.954
5	w	2	5w2	20.944
5	w	3	5w3	20.940
6	c	1	6c1	20.947
6	w	1	6w1	20.947
7	w	1	7w1	20.936

Analysis

The data were analyzed by fitting functions representing one of the models described earlier. In addition we compared the results with two "phonons only" fits to see whether including a vacancy contribution would indeed improve the description of the data by phonons alone. The four fitting functions we used are

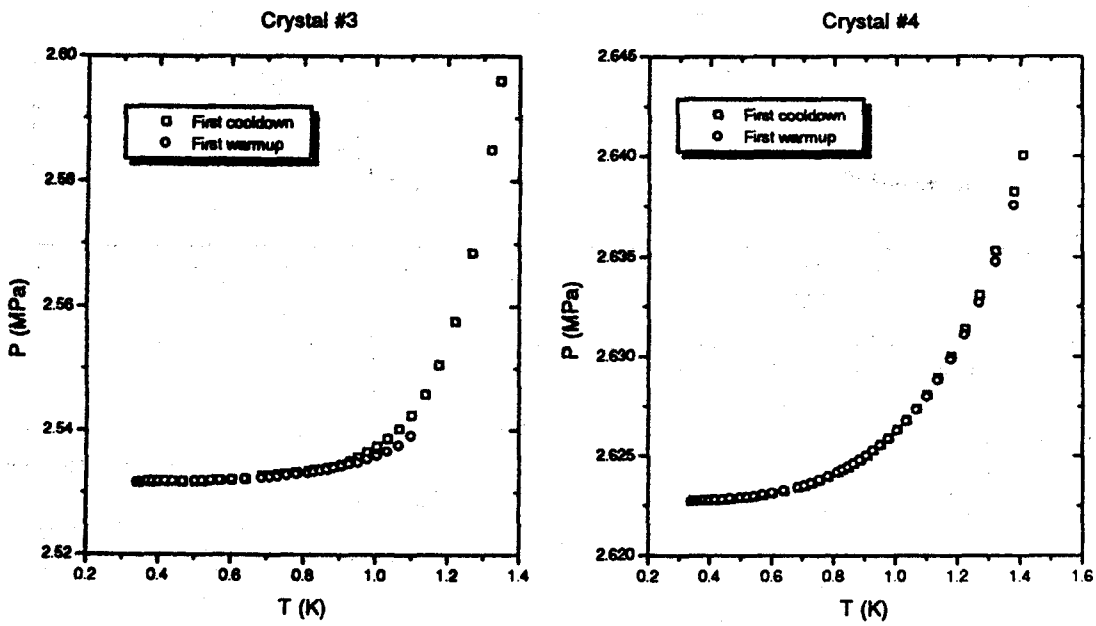

Fig. 4. The pressure of crystals Nos. 3 and 4 as a function of temperature. The reproducibility between a cool-down and a subsequent warm-up is good for No 4 but rather poor for No 3. The latter could be caused by inhomogeneities in the crystal, introduced during its growth.

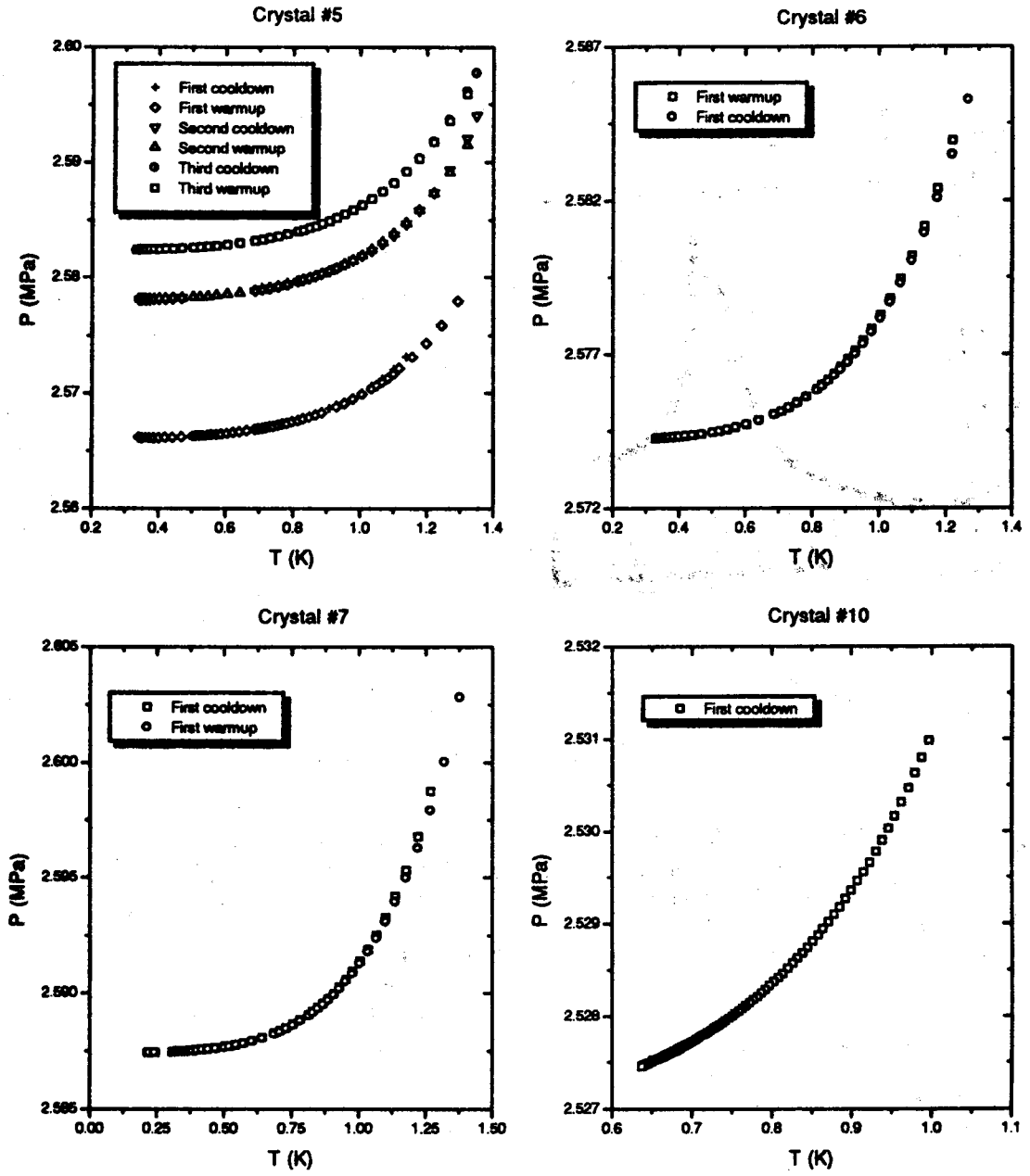

Fig. 5. Continuation of Fig. 4. The pressure as a function of temperature for crystals Nos. 5, 6, 7, and 10. All crystals show good reproducibility. The change in pressure for No 5 is due to a change in density at high temperatures.

$$P = P_0 + a_1 T^4 + a_2 T^6 + a_3 T^8 \text{ , phonons,} \quad (20)$$

$$P = P_0 + a_1 T^4 + a_2 T^8 + a_3 T^{10} \text{ , phonons (Gardner),} \quad (21)$$

$$P = P_0 + a_1 T^4 + a_2 \, e^{-a_3/T} \text{ , localized vacancies,} \quad (22)$$

$$P = P_0 + a_1 T^4 + a_2 T^{5/2} g_{5/2}(e^{-a_3/T}) \text{ , free vacancies.} \quad (23)$$

As one can see, we chose to use the same number of fit parameters in all functions for the obvious reason that a greater number of parameters will increase the degrees of freedom and automatically lead to a better fit, which makes quantitative analysis of the fit deviations impossible.

Phonons

The first and second coefficient of all fits (P_0 and a_1) show basically the same values, regardless of the type of fit. This is indicative of the intrinsic meaning of these coefficients, P_0 being the limiting

zero temperature pressure; a_1 being the Debye type phonon contribution. As a consistency check we compared the T^4 phonon contribution to the specific heat measurements by Gardner et al. [16]. Their coefficients for the heat capacity A (as seen in Table 1 of the article) can be converted to our T^4 coefficient a_1 by using Eq. (19):

$$a_1 = 7.0 \cdot 10^5 \frac{A(V_m)}{V_m} \text{ [Pa/K}^4\text{]} , \qquad (24)$$

where A is given in J/(mole·K^4) and the molar volume V_m in cubic centimeters. The a_1 values for the various crystals and fits is shown in Fig. 6. The solid lines represent the A values by Gardner for the molar volumes of our crystals. The scatter in our a_1 coefficient is too large ($\simeq$ 5%) to determine a molar volume dependence, which only constitutes a 1% change in a_1 .

The values for crystals 3 and 4 are much lower than the expected values. This is due to the poor growing conditions for these early crystals. The conditions for the later crystals improved as we became more skilled in controlling the pressure during growth.

For the remaining crystals the agreement with the heat capacity data is good considering the scatter of 5%. An interesting observation is the fact that the fits which do not include a vacancy contribution are systematically below the two expected lines, while the fits, that do include a vacancy term, only show random scatter.

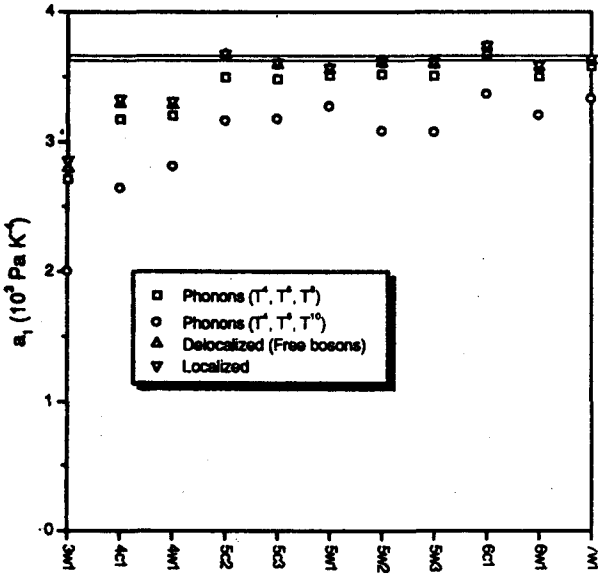

Fig. 6. The coefficient of the T^4 term for the various crystals and fits. Clearly to be seen is the improvement as a function of crystal number indicating better growth conditions. Also shown is the converted data (see text) by Gardner, indicated by the two solid lines.

Vacancies

Besides the phonon contribution we expect to find a vacancy term in the pressure. As we already indicated, it is possible that the phonon contribution, which can have T^6, T^8 and even T^{10} terms besides the usual T^4 term, will be indistinguishable from the exponential-like vacancy contribution. It is for this reason that we firstly compared fits with four free parameters containing only phonon terms (T^4, T^6, T^8 and T^4, T^8, T^{10}) and the limiting zero temperature pressure term (P_0) with other fourth order fits combining the lower order pressure and phonon terms (P_0 , T^4) with a vacancy contribution (free bosons).

It was found that for all crystals the standard deviation would be at least 2 times, but mostly an order of magnitude smaller when fitting vacancies to the experimental data, which means that our experimental precision clearly decides in favor of vacancies. More important, the deviation for the phonon fits from the data proved to be systematic, while the deviation of the vacancy fits only showed random scatter.

In Figs. 7 and 8 this can be clearly seen. Figure 7 shows deviations up to 200 Pa for the phonon fits, with a pressure resolution of $\simeq$ 0.4 Pa. The largest deviations are seen at the highest temperatures where the vacancy contribution is largest. Figure 8 shows the standard deviation for several fits.

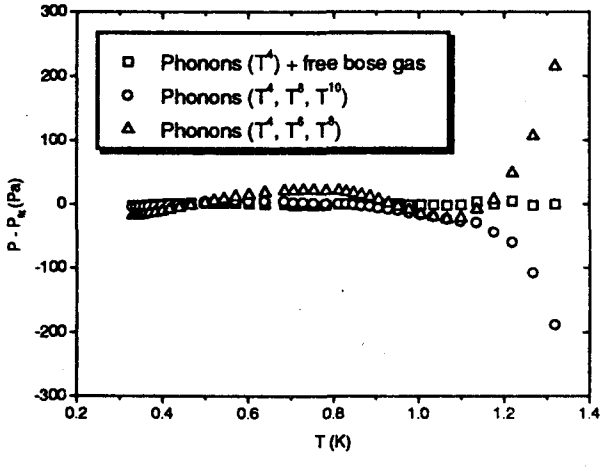

Fig. 7. The averaged data points of a P–T measurement with both phonon fits and a Bose gas fit subtracted are shown. The powers of T that are used in the phonon fits (see text) are indicated as well.

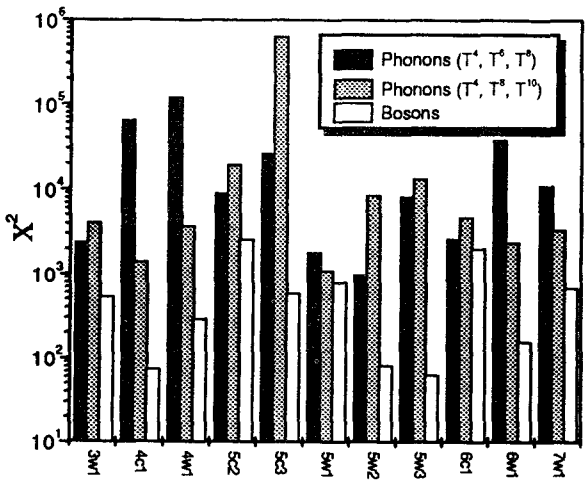

Fig. 8. The standard deviation of a vacancy (free boson) fit and different phonon fits summarized in a bar graph. Very clear is the large improvement gained from using vacancy fits. Please note the logarithmic y-scale.

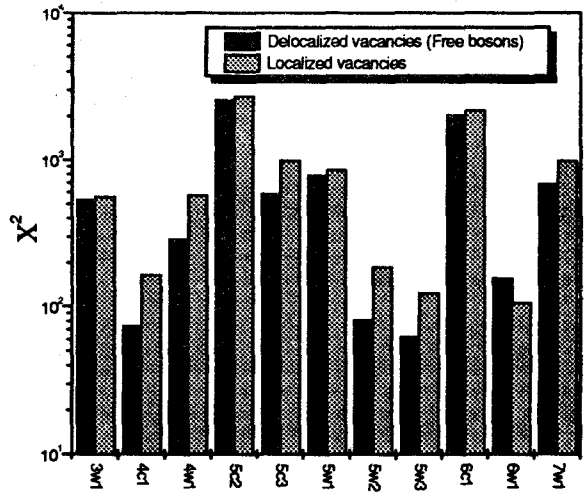

Fig. 9. A comparison between the standard deviation of localized and delocalized vacancy (free boson) fits. No clear difference can be seen although the delocalized vacancy fit seems to be slightly better.

Having established the presence of vacancies, a comparison was made between the localized model and the free Bose gas model. The standard deviation from the data is shown in Fig. 9. The models fit the data well, but within the experimental precision it is difficult to make a selection.

We must also bear in mind that, although a combination of a T^4 phonon term with a vacancy contribution fits the data better than a T^4, T^8 phonon term, the data of Gardner et al. suggests the presence of higher order phonon terms, which they proved by showing that the heat capacity followed a universal function of T/Θ for all molar volumes. It is possible however that a small part of the T^7 term is still due to vacancies. This could be within the experimental error, especially close to the melting temperature of his samples, where the data deviates considerably from the universal function. This implies that a fit containing both T^4, T^8 phonon and vacancy terms should be used, and that the magnitude of the higher order terms need not be as large as found by Gardner et al. [16].

Discussion

We will now discuss the merits of each model and the validity of the parameters that can be distilled from the fit coefficients. Because it is evident that the phonon part will include a T^8 term we extended the vacancy fits to incorporate this term as well. In order to restrict the number of free fit parameters the ratio of the T^4 and the T^8 coefficients was determined from Gardner's data, thus giving an upper limit on the phonon contribution.

The effect of introducing this additional term is illustrated in Fig. 10, where the activation energy is plotted for all crystals. Including the T^8 term decreases the magnitude of the energies but increases the scatter.

The fit coefficients for both models are summarized in Tables 2 and 3. The first and second coefficient P_0 and a_1 were discussed before. For the localized model the third and the last coefficient represent

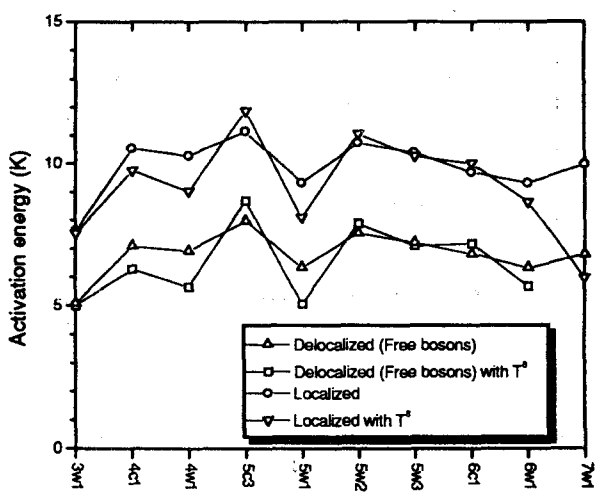

Fig. 10. Activation energy (a_3) as a function of crystal number for the localized and delocalized (free bosons) cases. The addition of the T^8 term decreases the coefficients by a small amount but increases the scatter significantly.

Table 2

The fit parameters for the localized and delocalized models (Bose gas) from Eqs. (24) and (25). The lowest row shows the averaged values for the last two coefficients

No	P_0, MPa	a_1, MPa·K^{-4}	a_2, MPa	a_3, K	P_0, MPa	a_1, MPa·K^{-4}	a_2, MPa·K$^{-5/2}$	a_3, K
	Localized vacancies				Delocalized vacancies (free bosons)			
3w1	2.5316	$2.853\cdot10^{3}$	2.731	7.608	2.5316	$2.788\cdot10^{3}$	0.2217	5.056
4c1	2.6227	$3.326\cdot10^{3}$	7.467	10.54	2.6227	$3.287\cdot10^{3}$	0.2830	7.090
4w1	2.6227	$3.309\cdot10^{3}$	4.957	10.27	2.6227	$3.281\cdot10^{3}$	0.2005	6.912
5c2	2.5780	$3.673\cdot10^{3}$	125.4	14.15	2.5780	$3.667\cdot10^{3}$	5.838	11.000
5c3	2.5824	$3.603\cdot10^{3}$	12.87	11.14	2.5824	$3.588\cdot10^{3}$	0.5914	7.972
5w1	2.5660	$3.568\cdot10^{3}$	2.306	9.334	2.5660	$3.551\cdot10^{3}$	0.1251	6.341
5w2	2.5780	$3.620\cdot10^{3}$	81.17	10.74	2.5780	$3.603\cdot10^{3}$	0.3720	7.558
5w3	2.5824	$3.611\cdot10^{3}$	6.561	10.39	2.5824	$3.590\cdot10^{3}$	0.3036	7.218
6c1	2.5742	$3.789\cdot10^{3}$	3.562	9.685	2.5742	$3.726\cdot10^{3}$	0.2141	6.821
6w1	2.5742	$3.585\cdot10^{3}$	2.676	9.308	2.5742	$3.566\cdot10^{3}$	0.1459	6.326
7w1	2.5874	$3.633\cdot10^{3}$	3.025	9.971	2.5874	$3.618\cdot10^{3}$	0.1389	6.787
Avg.	–	–	7.355	9.83	–	–	0.246	6.77

$$a_2 = N\left(\frac{\partial\Phi}{\partial V} - T\frac{\partial s}{\partial V}\right)e^{s/k_B}, \qquad (25)$$

a measure of the non-configurational entropy, and

$$a_3 = \Phi/k_B, \qquad (26)$$

the activation energy, respectively. Using the calculated values as shown in Table 2 in combination with the data of Lengua and Goodkind [17] for $N\partial\Phi/\partial V$, we find for the non-configurational entropy $s = -4.11k_B$. In that case, the vacancy concentration at the melting temperature of the crystals will be approximately $9\cdot10^{-6}$. Compared to the phonon entropy, which is $\simeq 3\cdot10^{-3}k_B$ per atom, such a large negative entropy per vacancy seems rather unphysical. In addition to that, the extremely low concentration is in clear disagreement with other work in which concentrations as high as

Table 3

The same table as before, but now the T^8 phonon term has been included, which lowers the vacancy terms and increases the scatter. The lower row contains averaged values for the vacancy coefficients

No	P_0, MPa	a_1, MPa·K^{-4}	a_2, MPa	a_3, K	P_0, MPa	a_1, MPa·K^{-4}	a_2, MPa·K$^{-5/2}$	a_3, K
	Localized vacancies				Delocalized vacancies (free bosons)			
3w1	2.5316	$2.829\cdot10^{3}$	2.292	7.525	2.5316	$2.768\cdot10^{3}$	0.1873	4.976
4c1	2.6227	$3.242\cdot10^{3}$	2.046	9.747	2.6227	$3.216\cdot10^{3}$	0.0788	6.283
4w1	2.6227	$3.233\cdot10^{3}$	7.385	9.042	2.6227	$3.215\cdot10^{3}$	0.0305	5.658
5c2	2.5780	$3.584\cdot10^{3}$	5349	19.89	–	–	–	–
5c3	2.5824	$3.541\cdot10^{3}$	10.72	11.87	2.5824	$3.535\cdot10^{3}$	0.4943	8.703
5w1	2.5660	$3.512\cdot10^{3}$	0.2751	8.106	2.5660	$3.501\cdot10^{3}$	0.0149	5.065
5w2	2.5780	$3.554\cdot10^{3}$	4.091	11.06	2.5780	$3.549\cdot10^{3}$	0.1900	7.891
5w3	2.5824	$3.546\cdot10^{3}$	2.529	10.25	2.5824	$3.538\cdot10^{3}$	0.1198	7.101
6c1	2.5742	$3.692\cdot10^{3}$	1.827	10.02	2.5742	$3.688\cdot10^{3}$	0.1124	7.180
6w1	2.5742	$3.533\cdot10^{3}$	0.6505	8.634	2.5742	$3.524\cdot10^{3}$	0.0367	5.680
7w1	2.5874	$3.558\cdot10^{3}$	0.0151	5.971	–	–	–	–
Avg.	–	–	4.467	9.54	–	–	0.126	6.49

0.1 to 1 percent were found [12,17]. This leads us to conclude that the localized model does not seem to be appropriate for the description of our results.

For the free Bose gas model the third coefficient can be interpreted as

$$a_2 = k_B^{5/2}\left(\frac{M}{2\pi\hbar^2}\right)^{3/2}, \qquad (27)$$

from which we can calculate the effective mass M of the vacancies by

$$\frac{M}{M_{^4\mathrm{He}}} = 1.32425\cdot 10^{-3} a_2^{2/3}. \qquad (28)$$

The last coefficient $a_3 = \Phi/k_B$ will again yield the activation energy. Table 4 summarizes the averaged results for both models.

The calculated values for the effective masses are larger than that of a bare ^{4}He atom. This is to be expected since the vacancy will not be able to move freely but will feel some interaction with the surrounding atoms. This interaction will reveal itself by the larger mass.

Table 4

The averaged physical properties as derived from the fit coefficients for both localized and delocalized models

	Localized		Delocalized (free bosons)		
	s/k_B, K	Φ/k_B, K	$M/M_{^4\mathrm{He}}$	Δ, K	Φ/k_B, K
T^4	−4.11±0.18	9.83±0.32	5.19±0.7	1.31±0.17	6.77±0.25
T^4, T^8	−4.61±0.33	9.54±0.55	3.58±0.9	2.05±0.47	6.49±0.43

In the tight binding approximation ($\Delta >> T$), the bandwidth can be determined from the effective mass with equation Eq. (15). From Table 4 it can be seen that the bandwidth is of the order of 1.3–2.1 K, which again indicates that the vacancies are only partly delocalized. This also means that a description in terms of free bosons is not completely valid, since the condition $\Delta >> T$ is not quite met.

In the limit that the activation energy is much larger than the temperature and the bandwidth ($\Phi >> \Delta, T$), a condition which is fulfilled in our case, the free Bose gas model, with the effective mass replaced by the bandwidth according to (15), is equivalent to a band model [19,20]. The values for the bandwidth given in table for the tight binding approximation are therefore equal to the values that would have been obtained using this bandwidth model.

Lengua and Goodkind [17] determined the molar volume dependence of the activation energy. On the bases of their data we expect $\Phi = 4$ K for the molar volumes investigated by us, which is much lower than the values we actually found. The discrepancy can be explained by the fact that the crystals grown by Lengua and Goodkind may have contained a much lower concentration of dislocations than ours. Since dislocations or strains in the crystals will have a localizing effect on the vacancies, this will yield an increase in both the effective mass and the energy of formation.

Another source of error could be the assumptions we have to make on the phonon contribution. This might seem worse than it actually is because we only assumed a certain functional behavior (T^4 and T^8). The magnitude of the phonon contribution is still fitted and determined within our experiment. It is for this reason that we expect these errors to be of minor importance.

5. Conclusions

We have shown that it is possible to detect the presence of vacancies by measuring the P–T relation of a crystal. It was found that the phonon contribution to the pressure is in good agreement with heat capacity measurements by Gardner et al. [16]. The additional vacancy term proved to be quite small and its magnitude depends on the assumptions one has to make on the phonon contribution. Within the framework of the free Bose gas model we have determined the effective mass of the vacancies, which was 3–5 times the bare mass of a ^{4}He atom, corresponding to a bandwidth of 1.3–2.1 K.

It was found that the crystal quality improves more by thermally cycling than by isothermal annealing. Activation energies, higher than measured by other authors were found, indicating that our samples may have contained a high concentration of dislocations. Improved measurements of, for instance, the heat capacity combined with simultaneous pressure measurements, and ultrasound measurements to consider crystal quality, would clarify these conflicting results.

This investigation was financially supported by Stichting FOM, which is part of the NWO in The Netherlands.

1. A. F. Andreev and I. M. Lifshitz, *Sov. Phys. JETP* **29**, 1107 (1969).
2. D. S. Greywall, *Phys. Rev.* **B18**, 2127 (1978); *Phys. Rev.* **B21**, 1329 (1978).
3. D. J. Bishop, M. A. Paalanen, and J. D. Reppy, *Phys. Rev.* **B24**, 2844 (1981).
4. G. Bonfait, H. Godfrin, and B. Castaing, *Proc. Quantum fluids and solids, AIP Conf. Proc.* **194**, 294 (1989).
5. M. W. Meisel, *Physica* **B178**, 121 (1992).
6. P. G. van de Haar, C. M. C. M. van Woerkens, M. W. Meisel, and G. Frossati, *J. Low Temp. Phys.* **86**, 349 (1992).

7. A. I. Shalnikov, *Sov. Phys. JETP* **20**, 1161 (1965).
8. K. O. Keshishev, L. P. Mezhov-Deglin, and A. I. Shal'nikov, *Sov. Phys. JETP Lett.* **12**, 160 (1970).
9. G. A. Sai-Halasz and A. J. Dahm, *Phys. Rev. Lett.* **28**, 124 (1972).
10. D. Marty and F. I. B. Williams, *J. Physique* **34**, 989 (1973).
11. K. O. Keshishev, *Sov. Phys. JETP* **45**, 273 (1977).
12. B. A. Fraass, P. R. Granfors, and R. O. Simmons, *Phys. Rev.* **B39**, 124 (1989).
13. A. R. Allen, M. G. Richards, and J. Schratter, *J. Low Temp. Phys.* **47**, 289 (1982).
14. V. N. Grigor'ev, B. N. Esel'son, and V. A. Mikheev, *Sov. J. Low. Temp. Phys.* **1**, 1 (1975).
15. T. Mizusaki, Y. Hirayoshi, S. Maekawa, and A. Hirai, *Phys. Lett.* **50A**, 160 (1974).
16. W. R. Gardner, J. K. Hoffer, and N. E. Phillips, *Phys. Rev.* **A7**, 1029 (1973).
17. G. A. Lengua and J. M. Goodkind, *J. Low Temp. Phys.* **79**, 251 (1990).
18. C. A. Burns and J. M. Goodkind, *J. Low Temp. Phys.* **95**, 695 (1994).
19. N. Sullivan, G. Deville, and A. Landesman, *Phys. Rev.* **B11**, 1858 (1975).
20. C. A. Burns, and J. M. Goodkind, *Physica* **B194-196**, 949 (1994).
21. Vespel, graphite filled polyimide, Dupont de Nemours.
22. XRP-5, 10 mm powder, manufactured by Comptoir Lyon Allemand Lonyot, 13 Rue Montmorency, Paris, France.
23. G. Frossati, *Ph. D. Thesis*, Grenoble (1978).
24. G. C. Straty and E. D. Adams, *Rev. Sci. Instr.* **40**, 1393 (1969).
25. 2850FT, manufactured by Emerson and Cummings, Canton, Massachusets 02021, U.S.A.
26. Degranges et Huot France, 10, rue Bernard-et-Mazoyer, 93300 Aubervilliers, France.
27. Andeen Hagerling, Inc. 31200 BainBridge Road, Cleveland Ohio 44139-2231 U.S.A.
28. J. F. Schooley, R. J. Soulen, and G. A. Evans, *Preparation and use of superconductive fixed point devices*, SRM 767 Issued by the National Bureau of Standards (1972).
29. E. R. Grilly, *J. Low Temp. Phys.* **11**, 33 (1973).
30. F. E. Moss, A. F. G. Wyatt, and M. J. Baird, *Cryogenics* **21**, 114 (1981).
31. P. V. E. McClintock, *Cryogenics* **18**, 201 (1978).
32. I. Iwasa and H. Suzuki, *J. Low Temp. Phys.* **62**, 1 (1986).